Efficient Construction of Nonorthogonal Localized Molecular Orbitals in Large Systems†

Ganglong Cui,‡,§ Weihai Fang,§ and Weitao Yang*,‡

Department of Chemistry, Duke University, Durham, North Carolina 27708, and Chemistry College, Beijing Normal University, Beijing 100875, China

Received: March 28, 2010; Revised Manuscript Received: May 27, 2010

Localized molecular orbitals (LMOs) are much more compact representations of electronic degrees of freedom than canonical molecular orbitals (CMOs). The most compact representation is provided by nonorthogonal localized molecular orbitals (NOLMOs), which are linearly independent but are not orthogonal. Both LMOs and NOLMOs are thus useful for linear-scaling calculations of electronic structures for large systems. Recently, NOLMOs have been successfully applied to linear-scaling calculations with density functional theory (DFT) and to reformulating time-dependent density functional theory (TDDFT) for calculations of excited states and spectroscopy. However, a challenge remains as NOLMO construction from CMOs is still inefficient for large systems. In this work, we develop an efficient method to accelerate the NOLMO construction by using predefined centroids of the NOLMO and thereby removing the nonlinear equality constraints in the original method (*J. Chem. Phys.* **2004**, *120*, 9458 and *J. Chem. Phys.* **2000**, *112*, 4). Thus, NOLMO construction becomes an unconstrained optimization. Its efficiency is demonstrated for the selected saturated and conjugated molecules. Our method for fast NOLMO construction should lead to efficient DFT and NOLMO-TDDFT applications to large systems.

1. Introduction

Since the first linear-scaling method of divide and conquer (DAC) was developed,[1,2] linear-scaling techniques have been widely and successfully applied to ab initio electronic structure calculations, first-principles molecular dynamics (MD) simulations, and quantum mechanics/molecular mechanics (QM/MM) modeling.[1−18] Development of linear-scaling techniques, in particular for excited states, remains an active area of electronic structure theory. With sparse matrix techniques, linear-scaling calculations can be achieved by means of DAC-style fragment methods, localized molecular orbitals (LMOs), and density matrices.[11,13,15−17,19−27]

In contrast to canonical molecular orbitals (CMOs), LMOs can accommodate more localized distributions for electrons in space, which is important for reducing the computational effort in the linear-scaling algorithms. LMOs can be represented either by NOLMOs or by orthogonal localized MOs (OLMOs).[28−30] Compared with NOLMOs, OLMOs have been extensively investigated and have a long history.[29,31,32] OLMOs can be obtained through unitary transformations from CMOs based on some localization criterion, such as Boys−Foster,[29] Edmiston−Ruedenberg,[21,22,31] Pipek−Mezey,[33] and Von Niessen schemes.[32] In addition, they can also be obtained using some particular schemes, for instance, the sparse coefficient space method based on the l_1-norm sparseness function,[9] the direct method without CMOs,[34] the "on the fly" localization method with 2×2 Jacobi rotations,[35] the isopycnic transformation of Cioslowski,[36] and the damped dynamical minimization method based on the spread object function in the context of Car−Parrinello molecular dynamics.[37]

Nevertheless, NOLMOs have not gained as much attention as OLMOs until recently.[28,30,38] Recent studies demonstrated that NOLMOs could achieve more compact/localized LMOs than OLMOs, with reduction in the spread function by about 10−28%.[28,38] This advantage stems from the release of orthogonal constraints, which removes the tails of OLMOs, resulting in more localized distributions of electrons in space. Another characteristic of NOLMOs is that the construction from CMOs is a highly parallel algorithm, because the construction for each NOLMO is independent of all other NOLMOs. Thus it is more efficient than OLMO construction where orthogonal constraints need to be satisfied.

Recently, linear-scaling calculations of ground and excited states with NOLMOs have been explored using the Hartree−Fock (HF), self-consistent charge density functional tight-binding (SCC-DFTB), and quantum Monte Carlo (QMC) methods.[10,27,39] The ground-state calculations not only demonstrate that NOLMOs are more compact/localized in space than OLMOs but also illustrate that accurate results can be achieved with smaller cutoff radii. Moreover, solution of the time-domain NOLMO-TDDFT equations, with low-scaling effort, was also investigated where NOLMO construction is repeatedly performed to maintain the sparsity of NOLMOs in a system.[27] The performance of these methods heavily rests on the efficiency of NOLMO construction in large systems.[10,27]

However, the original NOLMO construction is inefficient and might fail in large systems because of its four nonlinear equality constraints and the need of Boys centroids prior to NOLMO construction.[28] Furthermore, we believe that the unconstrained optimization algorithms will be more efficient than the constrained ones because the optimization techniques with nonlinear equality constraints are less mature than the unconstrained ones. The need of Boys centroids prior to NOLMO construction is another bottleneck preventing NOLMO applications to large systems. OLMO construction itself is inefficient in large systems, which is rooted in the successive 2×2 rotation

† Part of the "Klaus Ruedenberg Festschrift".

* To whom correspondence should be addressed. E-mail: weitao.yang@duke.edu.

‡ Duke University.

§ Beijing Normal University.

10.1021/jp1027838
Published on Web 06/15/2010

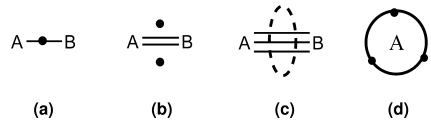

Figure 1. Illustration for NOLMO centroids in a single (a), double (b), and triple bond (c) and (d). (d) is a projection of the triple bond along the bond. The dots represent the centroids of corresponding orbitals.

operations needed to maintain the orthogonal conditions among OLMOs. In fact, OLMO construction is not a necessary step for constructing NOLMOs. Boys localization in the original method is only used to calculate the centroids of OLMOs. Imposing the condition that the centroids of NOLMOs are the same as the ones of OLMOs avoids linear dependence among NOLMOs. Localization of the centroids not only increases the computational effort but also introduces the nonlinear equality constraints in the original method. Therefore, it is significant to design an algorithm that is independent of OLMO construction and without any constraints. Specifically, we need an unconstrained algorithm for NOLMO construction in large systems.

On the basis of our observation of NOLMOs,[28] we found that the centroid of a MO representing a single bond is located in the middle of this bond. A double bond has two NOLMOs that form a set of "banana" bonds with centroids symmetrically located on the two sides of the double-bond plane. Correspondingly, the centroids of a triple bond are located at points spaced at 0, 120, and 240° around the cylinder's central plane, as shown in Figure 1.

With this "empirical" or "chemical intuition" selection of NOLMO centroids, OLMO construction can be avoided and the linear independence of NOLMOs can be satisfied by choosing the different centroids according to the above simple rules. In this work, we present the detailed formulations, implementations, results, and discussion of this improved NOLMO construction. We believe that this development will make NOLMO applications much more efficient, especially in large systems. The paper is divided into several parts with Method in section 2, Results and Discussion in section 3, and Conclusion in section 4.

2. Method

The main challenge in constructing NOLMOs from CMOs is finding a nonsingular transformation matrix **A**, which transforms CMOs into NOLMOs on the basis of eq 1

$$\psi_i = \sum_{k=1}^{n} A_{ki}\phi_k \tag{1}$$

where ψ_i is the ith NOLMO, ϕ_k is the kth CMO, and n is the number of the occupied MOs of a system. As the orthogonality conditions among MOs have been removed in constructing NOLMOs, the **A** matrix is not necessarily unitary and a nonsingular matrix is sufficient. In the course of construction, there are two conditions to be satisfied: NOLMO normalization $\Sigma_{k=1}^{n} A_{ik}^2 = 1$ and linear independence among NOLMOs. Correspondingly, the same scheme could be used to relocalize less-localized NOLMOs into more-localized ones, as done in recent work.[27] The transformation equation is

$$\psi_i = \sum_{k=1}^{n} A_{ki}\psi'_k \tag{2}$$

in which ψ'_k is the kth less-localized NOLMO, ψ_i is the ith more-localized NOLMO, and **A** remains a nonsingular matrix.

To present our method, some brief discussion on the original method is needed.[28] The original spread object function is defined as follows:

$$\Omega[\psi] = \sum_{k=1}^{n} \langle \psi_k | (\hat{\mathbf{r}} - \bar{\mathbf{r}})^2 | \psi_k \rangle \tag{3}$$

where $\hat{\mathbf{r}}$ is the electron position operator and $\bar{\mathbf{r}}$ is its expectation value for each NOLMO. In certain conditions, (3) can be traced back to the Boys localization scheme. In the Boys localization scheme, the minimization of Ω is realized by successive 2×2 unitary transformations, which satisfy the orthogonality conditions. As a result of the cross dependence in OLMO construction, it is inefficient in large systems. In contrast, there is no cross dependence in NOLMO construction because there is no orthogonal constraint. In the original NOLMO construction, the linear independence among NOLMOs is satisfied by choosing different centroids, which are obtained by means of Boys localization. Nevertheless, this prior localization drastically increases the computational effort, especially for large systems. Additionally, Boys localization remains inefficient in large systems. Finally, in the original method, the linear independence among NOLMOs is achieved by using nonlinear equality constraints in the object function, which imposes that the different NOLMO uses the different centroid. Generally, optimizations with nonlinear equality constraints are not as efficient as unconstrained optimizations. Hence, designing NOLMO construction with unconstrained algorithms is important and useful for NOLMO applications to large systems.

In this work, an unconstrained minimization method for NOLMO construction is proposed, which removes the nonlinear equality constraints in the original method.[28] The spread object function is defined as

$$\Omega[\psi] = \sum_{k=1}^{n} \frac{\langle \psi_k | (\hat{\mathbf{r}} - \mathbf{r}_k^0)^2 | \psi_k \rangle}{\langle \psi_k | \psi_k \rangle} \tag{4}$$

in which $\mathbf{r}_k^0 = \{x_k^0, y_k^0, z_k^0\}$ is the predetermined centroid (vector) of the kth NOLMO. In this spread object function, normalization constraints among NOLMOs are imposed explicitly through the denominator of eq 4 instead of the nonlinear equality constraints in the original method. The linear independence is satisfied by choosing different, but predetermined, centroids of NOLMOs, $\mathbf{r}_k^0 = \{x_k^0, y_k^0, z_k^0\}$. This modification makes NOLMO construction an unconstrained minimization process. Once the unconstrained minimization object functional, eq 4, is selected, many available procedures can be used to fulfill this minimization, for instance, the conjugated gradient, or quasi-Newton methods.

The simplification in the selection of NOLMO centroids is another important point in this work. Here we give up complicated and expensive operations and use an "empirical" or "chemical intuition" method to choose NOLMO centroids $\mathbf{r}_k^0 = \{x_k^0, y_k^0, z_k^0\}$ as explained in the Introduction (Figure 1). Different centroids for different NOLMOs ensure linear independence among NOLMOs.

Expressing the new spread object function Ω (eq 4) in terms of the transformation matrix, we have

$$\Omega[\mathbf{A}] = \sum_{k=1}^{n} \Omega_k[\mathbf{a}_k] \tag{5}$$

$$\Omega_k[\mathbf{a_k}] = [\mathbf{a}_k^\dagger \mathbf{R}^2 \mathbf{a}_k - 2(\mathbf{x}_k^0(\mathbf{a}_k^\dagger \mathbf{X}\mathbf{a}_k) + \mathbf{y}_k^0(\mathbf{a}_k^\dagger \mathbf{Y}\mathbf{a}_k) + \mathbf{z}_k^0(\mathbf{a}_k^\dagger \mathbf{Z}\mathbf{a}_k)) + (\mathbf{x}_k^0 x_k^0 + \mathbf{y}_k^0 y_k^0 + \mathbf{z}_k^0 z_k^0)(\mathbf{a}_k^\dagger \mathbf{a}_k)]/\mathbf{a}_k^\dagger \mathbf{a}_k \tag{6}$$

where $\mathbf{a_k}$ is the kth column vector of matrix $\mathbf{A}$ corresponding to the NOLMO ψ_k, and

$$(\mathbf{R}^2)_{ij} = \langle \phi_i | \hat{\mathbf{r}}^2 | \phi_j \rangle = \langle \phi_i | \hat{x}^2 + \hat{y}^2 + \hat{z}^2 | \phi_j \rangle \tag{7}$$

$$(\mathbf{R})_{ij} = \langle \phi_i | \hat{\mathbf{r}} | \phi_j \rangle \tag{8}$$

Note that the $\mathbf{R}$ matrix has three components $\mathbf{X}$, $\mathbf{Y}$, and $\mathbf{Z}$, and $\mathbf{r}_k^0 = \{x_k^0, y_k^0, z_k^0\}$ is the set of fixed centroids, preselected on the basis of chemical intuition, as shown in Figure 1. Equation 6 is the optimization object function for transforming CMOs into NOLMOs, which uses the orthogonal conditions among CMOs, $\langle \phi_i | \phi_j \rangle = \delta_{ij}$. If less-localized NOLMOs are transformed into more-localized ones, the overlap matrix of the less-localized NOLMOs would emerge in the equation

$$\Omega_k[\mathbf{a_k}] = [\mathbf{a}_k^\dagger \mathbf{R}^2 \mathbf{a}_k - 2(\mathbf{x}_k^0(\mathbf{a}_k^\dagger \mathbf{X}\mathbf{a}_k) + (\mathbf{y}_k^0(\mathbf{a}_k^\dagger \mathbf{Y}\mathbf{a}_k) + (\mathbf{z}_k^0(\mathbf{a}_k^\dagger \mathbf{Z}\mathbf{a}_k)) + (\mathbf{x}_k^0 x_k^0 + \mathbf{y}_k^0 y_k^0 + \mathbf{z}_k^0 z_k^0)(\mathbf{a}_k^\dagger \mathbf{S}\mathbf{a}_k)]/(\mathbf{a}_k^\dagger \mathbf{S}\mathbf{a}_k) \tag{9}$$

where

$$(\mathbf{S})_{ij} = \langle \psi_i' | \psi_j' \rangle \tag{10}$$

ψ_i' is the ith less-localized NOLMO and

$$(\mathbf{R}^2)_{ij} = \langle \psi_i' | \hat{\mathbf{r}}^2 | \psi_j' \rangle = \langle \psi_i' | \hat{x}^2 + \hat{y}^2 + \hat{z}^2 | \psi_j' \rangle \tag{11}$$

$$(\mathbf{R})_{ij} = \langle \psi_i' | \hat{\mathbf{r}} | \psi_j' \rangle \tag{12}$$

Finally, NOLMO construction can be transformed into optimization of the column vector $\mathbf{a_k}$ of the transformation matrix $\mathbf{A}$, as shown in eqs 6 and 9. This optimization is efficient and highly parallel since there is no cross dependence among the NOLMOs.

To perform minimization of eqs 6 and 9 efficiently with available optimization methods, the analytical gradient vector, and sometimes the Hessian matrix, are needed. Expressions for the gradient vector are given here and those for the Hessian matrix are in the Appendix.

The first-order derivative of $\Omega[\mathbf{a}_k]$ (eq 6) that transforms CMOs into NOLMOs can be derived through simple mathematical operations as shown here:

$$\frac{\partial \Omega[\mathbf{a}_k]}{\partial \mathbf{a}_k} = [(2\mathbf{R}^2\mathbf{a}_k - 4(\mathbf{x}_k^0\mathbf{X} + \mathbf{y}_k^0\mathbf{Y} + \mathbf{z}_k^0\mathbf{Z})\mathbf{a}_k + 2(\mathbf{x}_k^0 x_k^0 + \mathbf{y}_k^0 y_k^0 + \mathbf{z}_k^0 z_k^0)\mathbf{a}_k)(\mathbf{a}_k^\dagger \mathbf{a}_k)]/(\mathbf{a}_k^\dagger \mathbf{a}_k)^2 - [2(\mathbf{a}_k^\dagger \mathbf{R}^2 \mathbf{a}_k - 2(\mathbf{x}_k^0(\mathbf{a}_k^\dagger \mathbf{X}\mathbf{a}_k) + \mathbf{y}_k^0(\mathbf{a}_k^\dagger \mathbf{Y}\mathbf{a}_k) + \mathbf{z}_k^0(\mathbf{a}_k^\dagger \mathbf{Z}\mathbf{a}_k)))\mathbf{a}_k]/(\mathbf{a}_k^\dagger \mathbf{a}_k)^2 - [2(\mathbf{x}_k^0 x_k^0 + \mathbf{y}_k^0 y_k^0 + \mathbf{z}_k^0 z_k^0)(\mathbf{a}_k^\dagger \mathbf{a}_k)\mathbf{a}_k]/(\mathbf{a}_k^\dagger \mathbf{a}_k)^2 \tag{13}$$

where $\mathbf{r}_k^0 = \{x_k^0, y_k^0, z_k^0\}$ is the set of fixed centroids preselected on the basis of chemical intuition (Figure 1) and the definitions of $\mathbf{R}^2$ and $\mathbf{R} = \{\mathbf{X}, \mathbf{Y}, \mathbf{Z}\}$ are the same as those in eqs 7 and 8. The first-order derivative of eq 9, transforming less-localized NOLMOs into more-localized NOLMOs, is

$$\frac{\partial \Omega[\mathbf{a}_k]}{\partial \mathbf{a}_k} = [(2\mathbf{R}^2\mathbf{a}_k - 4(\mathbf{x}_k^0\mathbf{X} + \mathbf{y}_k^0\mathbf{Y} + \mathbf{z}_k^0\mathbf{Z})\mathbf{a}_k + 2(\mathbf{x}_k^0 x_k^0 + \mathbf{y}_k^0 y_k^0 + \mathbf{z}_k^0 z_k^0)\mathbf{S}\mathbf{a}_k)(\mathbf{a}_k^\dagger \mathbf{S}\mathbf{a}_k)]/(\mathbf{a}_k^\dagger \mathbf{S}\mathbf{a}_k)^2 - [2(\mathbf{a}_k^\dagger \mathbf{R}^2 \mathbf{a}_k - 2(\mathbf{x}_k^0(\mathbf{a}_k^\dagger \mathbf{X}\mathbf{a}_k) + \mathbf{y}_k^0(\mathbf{a}_k^\dagger \mathbf{Y}\mathbf{a}_k) + \mathbf{z}_k^0(\mathbf{a}_k^\dagger \mathbf{Z}\mathbf{a}_k)))\mathbf{S}\mathbf{a}_k]/(\mathbf{a}_k^\dagger \mathbf{S}\mathbf{a}_k)^2 - [2(\mathbf{x}_k^0 x_k^0 + \mathbf{y}_k^0 y_k^0 + \mathbf{z}_k^0 z_k^0)(\mathbf{a}_k^\dagger \mathbf{S}\mathbf{a}_k)\mathbf{S}\mathbf{a}_k]/(\mathbf{a}_k^\dagger \mathbf{S}\mathbf{a}_k)^2 \tag{14}$$

where the definitions of $\mathbf{S}$, $\mathbf{R}^2$ and $\mathbf{R} = \{\mathbf{X}, \mathbf{Y}, \mathbf{Z}\}$ are also same as those in eqs 10−12.

We point out that there are situations where we cannot easily select the centroids, such as during a chemical reaction, or in a complex bonding environment. It should also possible to determine the centroids: we could use an LMO scheme (such as the Boys localization) applied only on a fragment-by-fragment basis instead of to the full molecule.[29,40] This approach for choosing centroids, not implemented here, can lead to an automatic procedure for any bonding chemical environment.

In this work, the SCC-DFTB method is employed to calculate the related physical variables, $\mathbf{R}^2$, $\mathbf{R}$, and $\mathbf{S}$.[41] In principle, all unconstrained minimization procedures can be used, but here only the limited-BFGS (L-BFGS) is used to test our method.[42] Extension to other electronic structure and minimization methods is feasible.

3. Results and Discussion

We tested our unconstrained optimization method of NOLMO construction on several saturated or conjugated molecules: $C_{60}H_{122}$, $C_{60}H_{62}$, $C_{200}H_{202}$, and $C_6H_5C_2H_2(C_6H_4C_2H_2)_{11}C_6H_5$ (abbreviation in this work: MOL).

The SCC-DFTB method was employed to calculate the related quantities, for instance, $\mathbf{R}^2$, $\mathbf{R}$, $\mathbf{S}$, and the initial CMOs.[41] This method explicitly considers only the valence-shell electrons and AOs, for example, the 2s and 2p atomic orbitals for elements in the second row of the periodic table. At the SCC-DFTB level, there are 362 AOs in $C_{60}H_{122}$, 302 AOs in $C_{60}H_{62}$, 1002 AOs in $C_{200}H_{202}$, and 486 AOs in MOL.

The selection of NOLMO centroids is based on the "empirical" rules mentioned in the Introduction. The centroid of a single bond (C—C and C—H bonds in this work) is the middle point of this chemical bond; a double bond forms a set of "banana" bonds, and thus their centroids are fixed on the two sides of π the plane, 1 Å away from the plane of C═C double bond. This selection is based on our observation on the original NOLMOs that the centroids are at about the position of 1 Å.[28] With this selection, OLMO construction in the original method is eliminated, saving computational effort and removing nonlinear equality constraints.

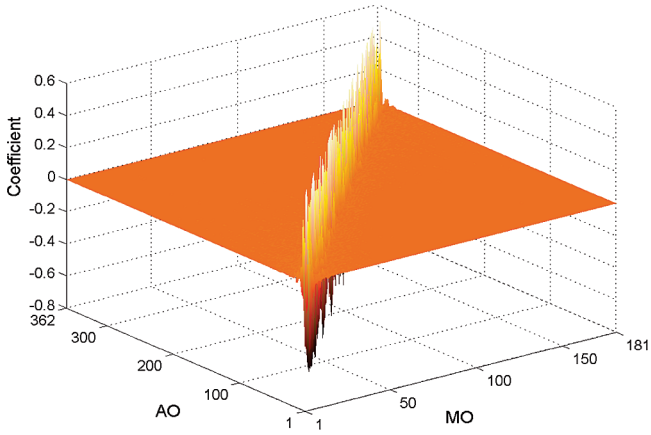

Figure 2. Sparsity distribution for NOLMOs in the saturated $C_{60}H_{122}$ molecule. The two abscissas stand for the AO/MO indexes, respectively, whereas the ordinate stands for the MO coefficient.

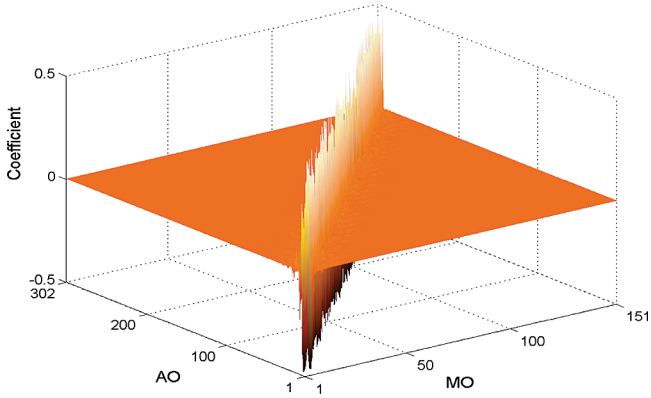

Figure 3. Sparsity distribution for NOLMOs in the unsaturated $C_{60}H_{62}$ molecule. The two abscissas stand for the AO/MO indexes, respectively, whereas the ordinate stands for the MO coefficient.

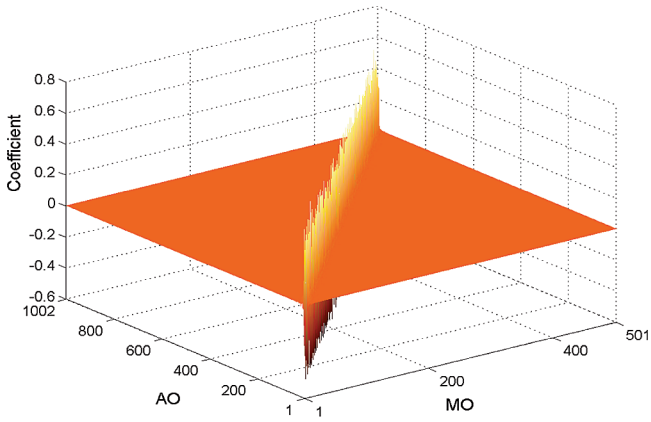

Figure 4. Sparsity distribution for NOLMOs in the unsaturated $C_{200}H_{202}$ molecule. The two abscissas stand for the AO/MO indexes, respectively, whereas the ordinate stands for the MO coefficient.

The NOLMO sparsity in large systems is illustrated by the 3-dimensional distribution plots, in Figures 2−5. In these plots, the abscissas represent the AO and MO indexes, whereas the ordinate is the MO coefficient. In all studied systems, the sparsity in AO space can be observed.

The sparsity in AO space exists not only in the saturated systems (Figure 2) but also in the conjugated systems (Figures 3−5). In terms of the sparse MO coefficient matrix, we can design and realize low-scaling or linear-scaling calculations of

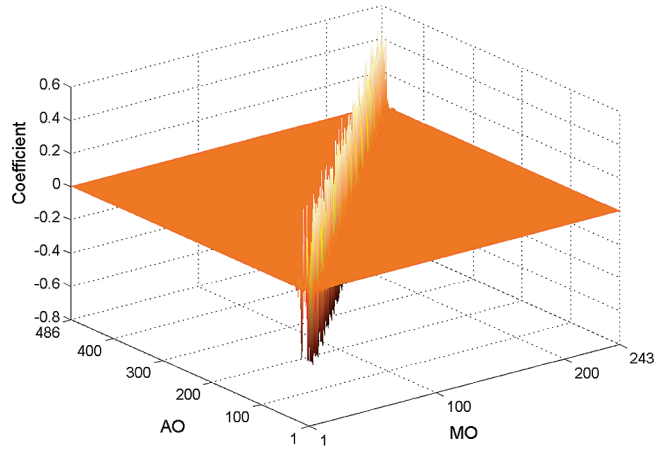

Figure 5. Sparsity distribution for NOLMOs in the unsaturated $C_6H_5C_2H_2(C_6H_4C_2H_2)_{11}C_6H_5$ molecule. The two abscissas stand for the AO/MO indexes, respectively, whereas the ordinate stands for the MO coefficient.

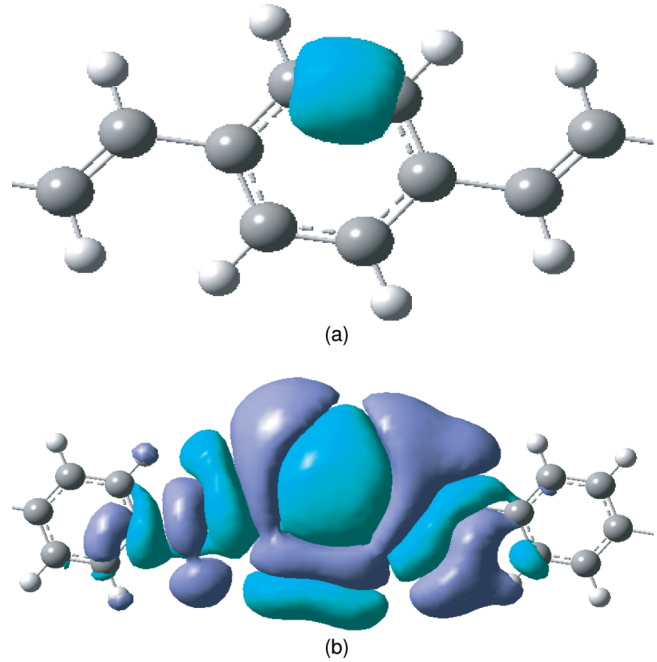

Figure 6. Real space representation for the 100th NOLMO (single bond) in a fragment of $C_6H_5C_2H_2(C_6H_4C_2H_2)_{11}C_6H_5$ molecule. The isosurface value is (1) (a) 0.1 and (b) 0.0001.

electronic structure, as demonstrated in recent linear-scaling or low-scaling calculations of ground and excited states in large systems.[10,27]

Additionally, NOLMO sparsity is reflected not only in AO space but also in real space. Here we chose one NOLMO to illustrate this property, for example, the 100th NOLMO of "MOL" plotted in Figure 6 with a 0.1 isosurface value and with a 0.0001 isosurface value. This NOLMO is localized in an extremely small portion of real space. A similar characteristic is also observed for other NOLMOs of the studied systems. This advantage can be used to reduce the computational effort of electronic structure calculations based on real-space grids.[43,44]

Compared with results of the original method, a similar NOLMO spread value for the C_6H_6 molecule is obtained: 35.5954 in the original method versus 37.2343 in the present work.[28] This small difference stems from the different centroids, electronic structure methods, basis sets, and spread object functions used in both methods. In principle, the unconstrained

algorithm of the present NOLMO construction is more efficient in large systems due to the removal of the nonlinear equality constraints and simple selection of NOLMO centroids. These improvements will make NOLMO construction avoid the OLMO construction and save computational effort.

4. Conclusion

With the unconstrained scheme presented in this paper, NOLMO construction in large systems becomes efficient. We remove the nonlinear equality constraints in the original method (refs 28 and 32) and simplify the selection of NOLMO centroids (Figure 1), which makes NOLMO construction an unconstrained minimization process. The efficiency of this method is demonstrated for both saturated and conjugated molecules. This improvement will make NOLMO-based DFT and TDDFT applications in large systems more efficient.[10,27]

Acknowledgment. Support from the National Scholarship Foundation of the Chinese Ministry of Education (G.C.) and from the National Science Foundation (W.Y.) is gratefully acknowledged.

Appendix: Analytical Hessian Matrices of Eqs 6 and 9

Before the second-order derivative of $\Omega[\mathbf{a}_k]$ in eq 6 is presented, some useful definitions are given for convenience. $\mathbf{o}_k$, $\mathbf{p}_k$, and $\mathbf{q}_k$ are defined as

$$\mathbf{o}_k = (2\mathbf{R}^2\mathbf{a}_k - 4(\mathbf{x}_k^0\mathbf{X} + \mathbf{y}_k^0\mathbf{Y} + \mathbf{z}_k^0\mathbf{Z})\mathbf{a}_k + 2(\mathbf{x}_k^0x_k^0 + \mathbf{y}_k^0y_k^0 + \mathbf{z}_k^0z_k^0)\mathbf{a}_k)\mathbf{a}_k^\dagger\mathbf{a}_k \quad (15)$$

$$\mathbf{p}_k = 2(\mathbf{a}_k^\dagger\mathbf{R}^2\mathbf{a}_k - 2(\mathbf{x}_k^0(\mathbf{a}_k^\dagger\mathbf{X}\mathbf{a}_k) + \mathbf{y}_k^0(\mathbf{a}_k^\dagger\mathbf{Y}\mathbf{a}_k) + \mathbf{z}_k^0(\mathbf{a}_k^\dagger\mathbf{Z}\mathbf{a}_k)) + (\mathbf{x}_k^0x_k^0 + \mathbf{y}_k^0y_k^0 + \mathbf{z}_k^0z_k^0)\mathbf{a}_k^\dagger\mathbf{a}_k)\mathbf{a}_k \quad (16)$$

$$q_k = (\mathbf{a}_k^\dagger\mathbf{a}_k)^2 \quad (17)$$

and thus eq 13 becomes $\partial\Omega[\mathbf{a}_k]/\partial\mathbf{a}_k = (\mathbf{o}_k - \mathbf{p}_k)/q_k$. Then, according to quotient derivative rules, we have

$$\frac{\partial^2\Omega[\mathbf{a}_k]}{\partial\mathbf{a}_k^{\,2}} = \frac{\left(\frac{\partial\mathbf{o}_k}{\partial\mathbf{a}_k} - \frac{\partial\mathbf{p}_k}{\partial\mathbf{a}_k}\right)q_k - (\mathbf{o}_k - \mathbf{p}_k)\frac{\partial q_k}{\partial\mathbf{a}_k}}{q_k^{\,2}} \quad (18)$$

where

$$\begin{aligned}\frac{\partial\mathbf{o}_k}{\partial\mathbf{a}_k} = {} & (2\mathbf{R}^2 - 4(\mathbf{x}_k^0\mathbf{X} + \mathbf{y}_k^0\mathbf{Y} + \mathbf{z}_k^0\mathbf{Z}) + 2(\mathbf{x}_k^0x_k^0 + \mathbf{y}_k^0y_k^0 + \mathbf{z}_k^0z_k^0)\mathbf{I})(\mathbf{a}_k^\dagger\mathbf{a}_k) + \\ & (2\mathbf{R}^2 - 4(\mathbf{x}_k^0\mathbf{X} + \mathbf{y}_k^0\mathbf{Y} + \mathbf{z}_k^0\mathbf{Z}) + 2(\mathbf{x}_k^0x_k^0 + \mathbf{y}_k^0y_k^0 + \mathbf{z}_k^0z_k^0)\mathbf{I})(\mathbf{a}_k\mathbf{a}_k^\dagger)\end{aligned} \quad (19)$$

$$\begin{aligned}\frac{\partial\mathbf{p}_k}{\partial\mathbf{a}_k} = {} & 2\mathbf{I}(\mathbf{a}_k^\dagger\mathbf{R}^2\mathbf{a}_k - 2(\mathbf{x}_k^0(\mathbf{a}_k^\dagger\mathbf{X}\mathbf{a}_k) + \mathbf{y}_k^0(\mathbf{a}_k^\dagger\mathbf{Y}\mathbf{a}_k) + \\ & \mathbf{z}_k^0(\mathbf{a}_k^\dagger\mathbf{Z}\mathbf{a}_k)) + (\mathbf{x}_k^0x_k^0 + \mathbf{y}_k^0y_k^0 + \mathbf{z}_k^0z_k^0)(\mathbf{a}_k^\dagger\mathbf{a}_k)) + \\ & 2\mathbf{a}_k\mathbf{a}_k^\dagger(2\mathbf{R}^2 - 4(\mathbf{x}_k^0\mathbf{X} + \mathbf{y}_k^0\mathbf{Y} + \mathbf{z}_k^0\mathbf{Z}) + \\ & 2(\mathbf{x}_k^0x_k^0 + \mathbf{y}_k^0y_k^0 + \mathbf{z}_k^0z_k^0)\mathbf{I})\end{aligned} \quad (20)$$

$$\frac{\partial q_k}{\partial\mathbf{a}_k} = 4\mathbf{a}_k^\dagger \quad (21)$$

Note that $\{\mathbf{r}_k^0\}$ is the set of fixed centroids selected on the basis of chemical intuition, as shown in Figure 1. The definitions of $\mathbf{R}^2$ and $\mathbf{R}$ are also same as those in eqs 7 and 8.

Analogously, the Hessian matrix of eq 9 is derived. It has the same mathematical form as eq 17 but different definitions for $\mathbf{o}_k$, $\mathbf{p}_k$, and $\mathbf{q}_k$. Here $\mathbf{o}_k$, $\mathbf{p}_k$, and $\mathbf{q}_k$ are

$$\mathbf{o}_k = (2\mathbf{R}^2\mathbf{a}_k - 4(\mathbf{x}_k^0\mathbf{X} + \mathbf{y}_k^0\mathbf{Y} + \mathbf{z}_k^0\mathbf{Z})\mathbf{a}_k + 2(\mathbf{x}_k^0x_k^0 + \mathbf{y}_k^0y_k^0 + \mathbf{z}_k^0z_k^0)\mathbf{S}\mathbf{a}_k)(\mathbf{a}_k^\dagger\mathbf{S}\mathbf{a}_k) \quad (22)$$

$$\mathbf{p}_k = 2(\mathbf{a}_k^\dagger\mathbf{R}^2\mathbf{a}_k - 2(\mathbf{x}_k^0(\mathbf{a}_k^\dagger\mathbf{X}\mathbf{a}_k) + \mathbf{y}_k^0(\mathbf{a}_k^\dagger\mathbf{Y}\mathbf{a}_k) + \mathbf{z}_k^0(\mathbf{a}_k^\dagger\mathbf{Z}\mathbf{a}_k)) + (\mathbf{x}_k^0x_k^0 + \mathbf{y}_k^0y_k^0 + \mathbf{z}_k^0z_k^0)(\mathbf{a}_k^\dagger\mathbf{S}\mathbf{a}_k))\mathbf{S}\mathbf{a}_k \quad (23)$$

$$q_k = (\mathbf{a}_k^\dagger\mathbf{S}\mathbf{a}_k)^2 \quad (24)$$

The definitions of $\mathbf{S}$, $\mathbf{R}^2$, and $\mathbf{R}$ are the same as those in eqs 10−12. The gradients of $\mathbf{o}_k$, $\mathbf{p}_k$, and $\mathbf{q}_k$ in eqs 21, 23, and 24 are

$$\begin{aligned}\frac{\partial\mathbf{o}_k}{\partial\mathbf{a}_k} = {} & (2\mathbf{R}^2 - 4(\mathbf{x}_k^0\mathbf{X} + \mathbf{y}_k^0\mathbf{Y} + \mathbf{z}_k^0\mathbf{Z}) + \\ & 2(\mathbf{x}_k^0x_k^0 + \mathbf{y}_k^0y_k^0 + \mathbf{z}_k^0z_k^0)\mathbf{S})(\mathbf{a}_k^\dagger\mathbf{S}\mathbf{a}_k) + \\ & (2\mathbf{R}^2 - 4(\mathbf{x}_k^0\mathbf{X} + \mathbf{y}_k^0\mathbf{Y} + \mathbf{z}_k^0\mathbf{Z}) + \\ & 2(\mathbf{x}_k^0x_k^0 + \mathbf{y}_k^0y_k^0 + \mathbf{z}_k^0z_k^0)\mathbf{I})\mathbf{a}_k(\mathbf{a}_k^\dagger\mathbf{S})\end{aligned} \quad (25)$$

$$\begin{aligned}\frac{\partial\mathbf{p}_k}{\partial\mathbf{a}_k} = {} & 2(\mathbf{a}_k^\dagger\mathbf{R}^2\mathbf{a}_k - 2(\mathbf{x}_k^0(\mathbf{a}_k^\dagger\mathbf{X}\mathbf{a}_k) + \mathbf{y}_k^0(\mathbf{a}_k^\dagger\mathbf{Y}\mathbf{a}_k) + \\ & \mathbf{z}_k^0(\mathbf{a}_k^\dagger\mathbf{Z}\mathbf{a}_k) + (\mathbf{x}_k^0x_k^0 + \mathbf{y}_k^0y_k^0 + \mathbf{z}_k^0z_k^0)(\mathbf{a}_k^\dagger\mathbf{S}\mathbf{a}_k))\mathbf{S} + \\ & 2\mathbf{S}\mathbf{a}_k\mathbf{a}_k^\dagger(2\mathbf{R}^2 - 4(\mathbf{x}_k^0\mathbf{X} + \mathbf{y}_k^0\mathbf{Y} + \mathbf{z}_k^0\mathbf{Z}) + \\ & 2(\mathbf{x}_k^0x_k^0 + \mathbf{y}_k^0y_k^0 + \mathbf{z}_k^0z_k^0)\mathbf{S})\end{aligned} \quad (26)$$

$$\frac{\partial q_k}{\partial\mathbf{a}_k} = 4\mathbf{a}_\mathbf{k}^\dagger\mathbf{S} \quad (27)$$

References and Notes

(1) Yang, W. T. *Phys. Rev. Lett.* **1991**, *66*, 1438.
(2) Yang, W. T. *J. Chem. Phys.* **1995**, *103*, 5674.
(3) York, D.; Lee, T.; Yang, W. T. *Phys. Rev. Lett.* **1998**, *80*, 5011.
(4) Yokojima, S.; Zhou, D. H.; Chen, G. H. *Chem. Phys. Lett.* **1999**, *302*, 495.
(5) Xiang, H. J.; Yang, J. L.; Hou, J. G.; Zhu, Q. S. *Phys. Rev. Lett.* **2006**, *97*, 266402.
(6) Xiang, H. J.; Yang, J. L.; Hou, J. G.; Zhu, Q. S. *J. Chem. Phys.* **2007**, *126*, 244707.
(7) Williamson, A. J.; Hood, R. Q.; Grossman, J. C. *Phys. Rev. Lett.* **2001**, *87*, 246406.

(8) Weber, V.; VandeVondele, J.; Hutter, J.; Niklasson, A. M. N. *J. Chem. Phys.* **2008**, *128*, 084113.
(9) Weber, V.; Hutter, J. *J. Chem. Phys.* **2008**, *128*, 064107.
(10) Burger, S. K.; Yang, W. T. *J. Phys. Condens. Matt* **2008**, *20*, 294209.
(11) Schutz, M.; Hetzer, G.; Werner, H. J. *J. Chem. Phys.* **1999**, *111*, 5691.
(12) Liang, W. Z.; Yokojima, S.; Chen, G. H. *J. Chem. Phys.* **1999**, *110*, 1844.
(13) Kohn, W. *Phys. Rev. Lett.* **1996**, *76*, 3168.
(14) Hernandez, E.; Gillan, M. J.; Goringe, C. M. *Phys. Rev. B* **1996**, *53*, 7147.
(15) Goedecker, S. *Rev. Mod. Phys.* **1999**, *71*, 1085.
(16) Galli, G. *Phys. Status Solidi B* **2000**, *217*, 231.
(17) Galli, G. *Curr. Opin. Solid State Mater. Sci.* **1996**, *1*, 864.
(18) Challacombe, M. *J. Chem. Phys.* **1999**, *110*, 2332.
(19) Bowler, D. R.; Gillan, M. J. *Comput. Phys. Com.* **1999**, *120*, 95.
(20) Niklasson, A. M. N.; Tymczak, C. J.; Challacombe, M. *J. Chem. Phys.* **2003**, *118*, 8611.
(21) Bytautas, L.; Ruedenberg, K. *Mol. Phys.* **2002**, *100*, 757.
(22) Bytautas, L.; Ivanic, J.; Ruedenberg, K. *J. Chem. Phys.* **2003**, *119*, 8217.
(23) Li, W.; Li, S. H. *J. Chem. Phys.* **2004**, *121*, 6649.
(24) Kobayashi, M.; Nakai, H. *J. Chem. Phys.* **2008**, *129*, 044103.
(25) Kobayashi, M.; Nakai, H. *J. Chem. Phys.* **2009**, *131*, 114108.
(26) Kobayashi, M.; Imamura, Y.; Nakai, H. *J. Chem. Phys.* **2007**, *127*, 074103.
(27) Cui, G. L.; Fang, W. H.; Yang, W. T. *Phys. Chem. Chem. Phys.* **2010**, *12*, 416.
(28) Feng, H.; Bian, J.; Li, L.; Yang, W. T. *J. Chem. Phys.* **2004**, *120*, 9458.
(29) Boys, S. F. *Rev. Mod. Phys.* **1960**, *32*, 296.
(30) Skylaris, C. K.; Mostofi, A. A.; Haynes, P. D.; Dieguez, O.; Payne, M. C. *Phys. Rev. B* **2002**, *66*, 035119.
(31) Edmiston, C.; Ruedenberg, K. *Rev. Mod. Phys.* **1963**, *35*, 457.
(32) Von Niessen, W. *J. Chem. Phys.* **1972**, *56*, 4290.
(33) Pipek, J.; Mezey, P. G. *J. Chem. Phys.* **1989**, *90*, 4916.
(34) Rubio, J.; Povill, A.; Malrieu, J. P.; Reinhardt, P. *J. Chem. Phys.* **1997**, *107*, 10044.
(35) VandeVondele, J.; Hutter, J. *J. Chem. Phys.* **2003**, *118*, 4365.
(36) Cioslowski, J. *Int. J. Quanum Chem.* **1990**, *S24*, 15.
(37) Iftimie, R.; Thomas, J. W.; Tuckerman, M. E. *J. Chem. Phys.* **2004**, *120*, 2169.
(38) Liu, S. B.; Perez-Jorda, J. M.; Yang, W. T. *J. Chem. Phys.* **2000**, *112*, 1634.
(39) Reboredo, F. A.; Williamson, A. J. *Phys. Rev. B* **2005**, *71*, 121105.
(40) Kitauraa, K.; Ikeoa, E.; Asadaa, T.; Nakanob, T.; Uebayasic, M. *Chem. Phys. Lett.* **1999**, *313*, 701.
(41) Elstner, M.; Frauenheim, T.; Kaxiras, E.; Seifert, G.; Suhai, S. *Phys. Status Solidi B* **2000**, *217*, 357.
(42) Nocedal, J. *Math. Comput.* **1980**, *35*, 773.
(43) Castro, A.; Appel, H.; Oliveira, M.; Rozzi, C. A.; Andrade, X.; Lorenzen, F.; Marques, M. A. L.; Gross, E. K. U.; Rubio, A. *Phys. Status Solidi B* **2006**, *243*, 2465.
(44) Yabana, K.; Nakatsukasa, T.; Iwata, J. I.; Bertsch, G. F. *Phys. Status Solidi B* **2006**, *243*, 1121.

JP1027838